Environmental Science & Technology

Article

pubs.acs.org/est

Iron Isotope Fractionations Reveal a Finite Bioavailable Fe Pool for Structural Fe(III) Reduction in Nontronite

Bingjie Shi,[†,‡] Kai Liu,[†,‡] Lingling Wu,*[,†,‡] Weiqiang Li,[§,∥] Christina M. Smeaton,[†,‡] Brian L. Beard,[§,∥] Clark M. Johnson,[§,∥] Eric E. Roden,[§,∥] and Philippe Van Cappellen[†,‡]

[†]Department of Earth and Environmental Sciences, University of Waterloo, Waterloo, Ontario N2L 3G1, Canada

[‡]Water Institute, University of Waterloo, Waterloo, Ontario N2L 3G1, Canada

[§]Department of Geoscience, University of Wisconsin-Madison, Madison, Wisconsin 53706, United States

[∥]NASA Astrobiology Institute, University of Wisconsin-Madison, Madison, Wisconsin 53706, United States

Supporting Information

ABSTRACT: We report on stable Fe isotope fractionation during microbial and chemical reduction of structural Fe(III) in nontronite NAu-1. $^{56}Fe/^{54}Fe$ fractionation factors between aqueous Fe(II) and structural Fe(III) ranged from −1.2 to +0.8‰. Microbial (*Shewanella oneidensis* and *Geobacter sulfurreducens*) and chemical (dithionite) reduction experiments revealed a two-stage process. Stage 1 was characterized by rapid reduction of a finite Fe(III) pool along the edges of the clay particles, accompanied by a limited release to solution of Fe(II), which partially adsorbed onto basal planes. Stable Fe isotope compositions revealed that electron transfer and atom exchange (ETAE) occurred between edge-bound Fe(II) and octahedral (structural) Fe(III) within the clay lattice, as well as between aqueous Fe(II) and structural Fe(III) via a transient sorbed phase. The isotopic fractionation factors decreased with increasing extent of reduction as a result of the depletion of the finite bioavailable Fe(III) pool. During stage 2, microbial reduction was inhibited while chemical reduction continued. However, further ETAE between aqueous Fe(II) and structural Fe(III) was not observed. Our results imply that the pool of bioavailable Fe(III) is restricted to structural Fe sites located near the edges of the clay particles. Blockage of ETAE distinguishes Fe(III) reduction of layered clay minerals from that of Fe oxyhydroxides, where accumulation of structural Fe(II) is much more limited.

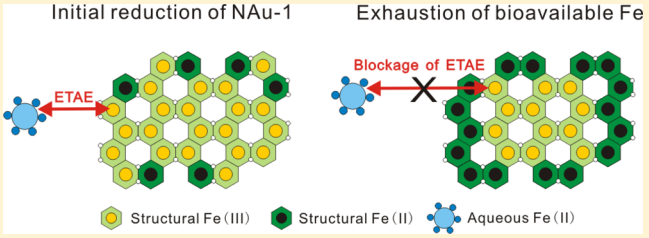

INTRODUCTION

Transformations of clay minerals in near-surface environments influence soil fertility, contaminant mobility, and hydrocarbon maturation.[1−4] Iron (Fe) is ubiquitous in clay minerals.[5,6] The oxidation state of structural Fe greatly influences the physical and chemical properties of clay minerals, including specific surface area, cation exchange capacity, structure and stability, as well as hydration and swelling.[6−9] These processes in turn determine the fate of contaminants such as metal cations,[10] radionuclides,[11] and organic contaminants.[12] Structural Fe(III) in clay minerals also represents a potentially renewable source of terminal electron acceptor for dissimilatory Fe(III)-reducing bacteria in soils and sediments, as Fe(III) in clay minerals is not subjected to reductive dissolution to the same extent as in Fe(III) oxyhydroxides.[13−15]

Although the importance of clay transformation by microbes has been recognized over the last two decades, the electron transfer and atom exchange pathways during reduction of structural Fe(III) in clays remain unclear.[16,17] Microbial reduction of Fe(III) in clays has been proposed to start from the edges and progress through the octahedral sheet as a moving front,[18] in contrast to a pseudorandom chemical reduction starting from the basal plane surfaces.[19] Two mechanisms for microbial reduction of Fe(III) in clays have further been suggested: solid-state and dissolution−precipitation, where the former refers to reduction within the clay structure without significant release of Fe(II) to the aqueous phase,[20,21] and the latter to dissolution of the clay structure and precipitation of secondary minerals.[15,22,23] Operation of either mechanism may depend on the clay mineral, growth medium composition, and the density and type of microorganisms.[17]

Stable Fe isotopes are a powerful tracer of biogeochemical processes involving redox transformations of Fe minerals.[24] Iron isotope compositions in natural environments span a range of up to 6‰ in $\delta^{56}Fe$ values (defined as the $^{56}Fe/^{54}Fe$ ratio of a sample relative to a reference material, such as igneous rocks),[25,26] with the largest variations observed in Precambrian marine sedimentary rocks.[24] Both biological and abiological processes can fractionate Fe isotopes, with the largest fractionations associated with redox changes.[27,28] Coupled electron and atom exchange has been shown to be

Received: April 25, 2016
Revised: June 10, 2016
Accepted: June 12, 2016
Published: June 13, 2016

DOI: 10.1021/acs.est.6b02019
Environ. Sci. Technol. 2016, 50, 8661−8669

Table 1. Experimental Design

experiments	setup	number of reactors	processes	presence of Fe(II)	electron transfer	atom exchange
abiotic control	NAu-1 + medium	1	nonreductive dissolution	no	no	yes
biological reduction	NAu-1 + medium + cells (*Shewallena*/*Geobacter*)	2 duplicates	reduction, dissolution (reductive and nonreductive)	yes	yes	yes
chemical reduction	NAu-1 + dithionite	6 individuals	reduction, dissolution (reductive and nonreductive)	yes	yes	yes
abiotic exchange	NAu-1 + Fe(II) (4:1 molar Fe ratio)	2 duplicates	exchange (equivalent to a fixed extent of reduction)	yes	yes	yes

the mechanism responsible for Fe isotope fractionation during microbial Fe(III) oxide reduction,[29−31] as well as during abiological interaction between aqueous Fe(II) and Fe(III) oxides.[32−34] Here, we use Fe isotope fractionations as a tracer to investigate atom exchange and changes in bonding that are produced by both microbial and chemical reduction of Fe-rich smectite NAu-1. A similar approach has proven valuable in understanding electron transfer and atom exchange (ETAE) pathways during reduction of structural Fe(III) in oxides/hydroxides. Notwithstanding extensive research on microbial and chemical reduction of structural Fe(III) in clay minerals,[15−23] no information currently exists on the partitioning of Fe isotopes during reduction of structural Fe(III) in clays. This study aims to provide new insights into ETAE pathways during reduction of structural Fe in clay minerals.

MATERIALS AND METHODS

Clay Mineral Preparation. Nontronite NAu-1 [$(Ca, Na, K)_{1.05}[Si_{6.98}Al_{1.02}][Al_{0.29}Fe_{3.68}Mg_{0.04}]O_{20}(OH)_4$] was obtained from the Clay Minerals Society[35] and further treated by a size-fractionation (<0.5 μm), Na^+-homoionization and purification process.[36,37] The purified nontronite was freeze-dried, pulverized and then sieved (100 mesh/150 μm). X-ray diffraction (XRD) and scanning electron microscopy (SEM) coupled to energy dispersive spectroscopy (EDS) analysis showed no evidence for the presence of impurities, such as goethite, quartz, or kaolin, in the purified NAu-1 (Supporting Information (SI) Figures S1 and S2).

Microbial and Chemical Reduction Experiments. An overview of the experimental design is given in Table 1, additional details can be found in SI Table S1. *Shewanella oneidensis* MR-1[38] was grown aerobically in LB media, prior to inoculation of the clay-bearing suspensions. Cells were harvested and washed twice with sterile HEPES buffer before adding 2×10^8 cells/mL to 120 mL of HEPES buffer (100 mM, pH 6.8) containing 5 mg/mL NAu-1 [Fe(III) electron acceptor], 40 mM Na-lactate (electron donor), 100 μM KH_2PO_4, and 5 mM $(NH_4)_2SO_4$. *Geobacter sulfurreducens* strain PCA[39] was incubated with fumarate (electron acceptor) and acetate (carbon and energy source) prior to inoculation. Cells were harvested and washed once with sterile, anaerobic PIPES buffer before adding 5×10^8 cells/mL to 120 mL anaerobic, H_2-saturated PIPES buffer (10 mM, pH 6.8) containing 5 mg/mL NAu-1. Acetate (final 20 mM) and the electron shuttle anthraquinone-2,6-disulfonate (AQDS, final 0.1 mM) were successively added to the *Geobacter* reactors 137 days and 155 days after initiating the experiments, respectively.

In order to maintain anaerobic conditions, the glass reactors were crimp sealed using gas impermeable butyl rubber stoppers, and shaken at 100 rpm. Duplicate biotic and abiotic (cell-free) control reactors were prepared. The pH values in the biotic reactors remained stable at 6.8 even after more than 400 days of incubation. Parallel abiotic reduction reactors were prepared by adding 15 to 200 mg sodium dithionite to 10 mL 100 mM HEPES buffer (pH 6.8) with NAu-1 (5 mg/mL) to achieve an analogous or greater extent of reduction as observed in the biotic reactors. The abiotic reactors were kept at room temperature, or at 70 °C to achieve a higher extent of reduction (SI Table S1). Limited reaction time was employed to avoid a much higher extent of reduction (i.e., 20 days for nearly 100% reduction as in a previous study[40]).

Exchange Experiments of Fe(II) with NAu-1. A ^{57}Fe-enriched Fe(II) stock solution ($\delta^{56/54}$Fe = −0.49‰ and $\delta^{57/56}$Fe = +104.83‰) was prepared by mixing a ^{57}Fe-enriched spike with a natural abundance Fe(II) solution at a molar ratio of ca. 1:500. Batch reactors contained 15 mL of 25 mM MES buffer adjusted to pH 6.0, 50 mM NaCl to provide a constant ionic strength, and 2 mM of ^{57}Fe-enriched aqueous Fe(II). The reaction was started by adding 30.0 mg of purified NAu-1 powder to the reactors.

Fe Extractions and Chemical Analysis. At selected time points during the reduction experiments, 10 mL of the clay suspensions were collected from each reactor and centrifuged (6500 rpm, 15 min). The supernatant was filtered (0.2 μm) to isolate the aqueous fraction. The remaining solid was extracted for 4 h with 1 M $CaCl_2$ (pH 7) to remove the Fe(II) sorbed on the clay mineral basal planes.[36] This extraction relies on the displacement of basal plane sorbed Fe^{2+}, including interlayer Fe^{2+}, by excess Ca^{2+}.[41] The mixture was centrifuged, filtered and acidified for preservation. Then the remaining solid was mixed with 5 mL 1 M NaH_2PO_4 (pH 5) for 18 h to isolate the Fe(II) sorbed to the clay mineral edge OH-groups.[36] This extraction is based on the high affinity of Fe−OH groups for phosphate ions.[42] In addition to edge-bound Fe(II), this extraction may also partially recover structural Fe(II).[33] The remaining solid was mixed with 5 mL 0.5 M HCl for 24 h to extract the residual structural Fe(II).[5] Note that 0.5 M HCl may also partially remove structural Fe(III). The mixture solution was centrifuged and filtered. For chemical reactors, the residual solid after the 0.5 M HCl extraction was further treated with 48% HF to quantify any remaining structural Fe(II).[43]

Iron(II) concentrations were determined spectrophotometrically using Ferrozine[44] for the reduction experiments and 1,10-phenanthroline[45] for the exchange experiments. Total Fe [Fe(tot)] was measured after addition of 10% hydroxylamine hydrochloride to reduce Fe(III). The Fe(III) concentration was then calculated as the difference of Fe(tot) and Fe(II). In the HF treatment, 1,10-phenanthroline monohydrate was used to form strong tris complexes with Fe(II) in the HF-H_2SO_4 matrix.[43] Next, H_3BO_4 and Na_2-citrate were added and the absorbance was measured at 510 nm. This method has been shown to quantitatively determine Fe(II) in silicate minerals.[43]

DOI: 10.1021/acs.est.6b02019
Environ. Sci. Technol. 2016, 50, 8661−8669

Aqueous silica concentrations were analyzed using a standard colorimetric method.[46]

Fe Isotope Analysis. Test solutions, used to check the accuracy of Fe isotope analyses, were prepared by adding 50 μg of HPS (high purity standard) Fe to 10 mL 100 mM HEPES buffer, 0.5 to 5 mL 1 M $CaCl_2$, 0.5 to 5 mL 1 M NaH_2PO_4, or 3 to 10 mL 2.5 to 15 mg/mL dithionite in order to identify potential Fe isotope fractionation artifacts produced during the chemical extractions or by the use of dithionite as chemical reductant. Wet chemistry was performed on the solutions to separate Fe from other cations by passing them through an anion-exchange resin.[47] Iron isotope compositions of the aqueous fractions, extracts and test solutions were measured by a multicollector, inductively coupled plasma mass spectrometer (MC-ICP-MS) at University of Wisconsin, Madison, following established protocols.[47] All Fe isotope data were reported as δ^{56}Fe in units of per mil (‰) relative to average terrestrial igneous rocks (δ^{56}Fe = 0.00 ± 0.05‰[47]). Stable Fe isotope fractionation between two phases A and B is defined as $\Delta^{56}Fe_{A\text{-}B} = \delta^{56}Fe_A - \delta^{56}Fe_B$, following standard practice. Measured external precision for δ^{56}Fe was ±0.05‰ (2σ, n = 37). The average δ^{56}Fe value of the test solutions was 0.50 ± 0.08‰ (2σ; n = 24), which is identical to the isotope composition measured for the pure HPS Fe solutions (δ^{56}Fe = 0.49 ± 0.06‰; 2σ; n = 27). The measured Fe isotope composition of the IRMM-019 Fe isotope standard was −0.08 ± 0.05‰ (2σ; n = 48), which lies within error of the long-term value in the UW-Madison lab of −0.09‰ relative to the average of igneous rocks.

RESULTS

Microbial and Chemical Reduction of NAu-1. Smectite has a 2:1 layer structure in which an octahedral sheet is bound by two tetrahedral sheets through sharing the apical oxygens.[48] Structural Fe(III) in NAu-1 (~22 wt %[35]) is located in the octahedral sheet with edge sites exposed to solution. Reduction of structural Fe(III) in the biological and chemical experiments was monitored by measuring Fe(II) in the aqueous phase and in the solutions produced by the three sequential wet-chemical extraction steps: i. 1 M $CaCl_2$, which quantitatively removes Fe(II) sorbed onto basal planes; ii. 1 M NaH_2PO_4, which releases Fe(II) bound to OH-group at edge sites and partial structural Fe(II); and iii. 0.5 M HCl, which removes structural Fe(II) and a portion of structural Fe(III). The Fe(II) and Fe(tot) data showed that Fe released to aqueous solution and Fe in the first two extractions were entirely comprised of Fe(II), while the 0.5 M HCl extracts contained a mixture of Fe(II) and Fe(III) (SI Table S2). In other words, structural Fe(III) is the only Fe(III) phase throughout our experiments. The selective release of basal plane sorbed Fe(II) and edge OH-group bound Fe(II) during the first two extractions has previously been confirmed by Mössbauer analysis of Fe(II)-reacted NAu-1 and the reference Fe-free montmorillonite SYn-1.[36] It is not possible to resolve whether edge-bound Fe(II) derives from in situ reduction or readsorbed Fe(II).

In the biological reduction experiments with *Shewanella* and *Geobacter*, Fe(II) concentrations increased with time (Figure 1, SI Table S2). Edge plus structural Fe(II) accounted for the largest fraction of biogenic Fe(II) (55–71%; SI Table S3, Figure S3), structural Fe(II) in the interior of the NAu-1 accounted for 13 to 21% of total produced Fe(II), and aqueous Fe(II) accounted for 4–12% total produced Fe(II). Only 2–7% of the Fe(II) released in the experiments with *Shewanella*

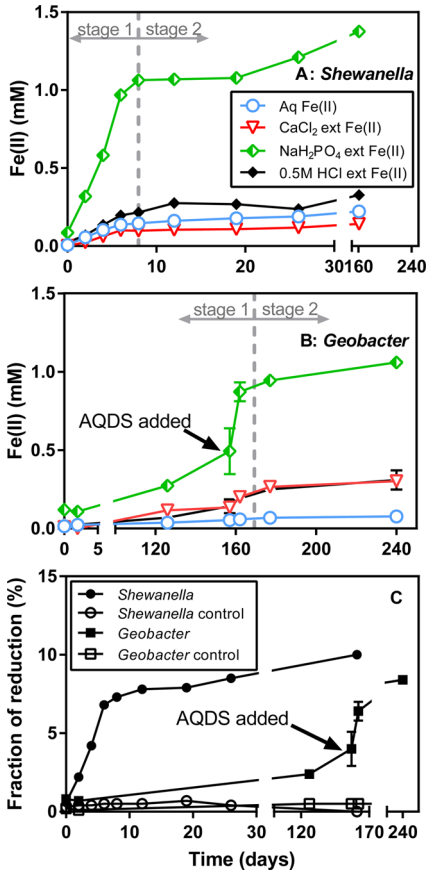

Figure 1. Time-dependent buildup of different Fe(II) pools during biological reduction of NAu-1 by *Shewallena* (panel A) and *Geobacter* (panel B). The pools include dissolved Fe(II), 1 M $CaCl_2$ extractable Fe(II) (basal planes), 1 M NaH_2PO_4 extractable Fe(II) (edge plus structural sites), and 0.5 M HCl extractable Fe(II) (interior sites). The electron shuttle AQDS was added after 155 days to the *Geobacter* reactors to facilitate reduction. The vertical gray lines indicate the transition from stage 1 to stage 2. The fraction of reduction was calculated as the total Fe(II) relative to the initial total Fe of NAu-1 (panel C). Error bars indicate one standard deviation from duplicate reactors. No reduction was observed in controls where no cells were present.

sorbed onto basal planes. During NAu-1 reduction by *Geobacter* in the presence of AQDS, a larger fraction (15–17%) of basal plane sorbed Fe(II) was observed. However, together aqueous and basal-sorbed Fe(II) accounted for a fairly constant fraction of the total Fe(II) produced by *Shewanella* and *Geobacter* (18 ± 2%, SI Table S3, Figure S3).

In the chemical reduction experiments (i.e., without bacteria), edge plus structural Fe(II) accounted for 54–64% of total Fe(II) (SI Table S3, Figure S3), similar to that of biological experiments. Interior structural Fe(II) accounted for 22–41% of total Fe(II) and showed an increasing trend with increasing extent of reduction. Compared to the biological reduction experiments, the larger fraction of interior structural Fe(II), for a comparable extent of reduction (SI Table S3, Figure S3), suggests that dithionite was able to reduce more of the interior pool of octahedral Fe(III), probably due to the small molecular size of dithionite (S–O and S–S bond length of 1.5 and 2.3 Å, respectively[49]), enabling it to diffuse into the clay interior through the basal planes (hexagonal cavity 2.7 Å[50]) (SI Figure S4C). Aqueous Fe(II) represented 4–13% of total

DOI: 10.1021/acs.est.6b02019
Environ. Sci. Technol. 2016, 50, 8661–8669

Fe(II), and basal-sorbed Fe(II) accounted for the smallest percentage (1−5%). Further HF treatment recovered less than 2% of total produced Fe(II), indicating that 0.5 M HCl was sufficient to recover all structural Fe(II) in our experiments.

Dissolved and sorbed silica concentrations indicated a maximum of 1.6% clay mineral dissolution (SI Figure S5), which is consistent with limited reductive dissolution of Fe-containing clays.[17] No Fe-bearing secondary minerals were observed (by SEM) on clay surfaces in biologically or chemically reduced NAu-1 after more than 400 days incubation (Figure S6, see SI for a detailed discussion).

Changes in Fe Isotope Composition during Microbial and Chemical Reduction. Significant changes in the Fe isotope compositions of the various Fe(II) and Fe(III) pools occurred during biological and chemical reduction (Figure 2, SI Table S4), with marked deviations from the starting bulk NAu-1 composition (δ^{56}Fe = 0.59‰). The δ^{56}Fe values for octahedral Fe(III) extracted by 0.5 M HCl were calculated by assuming that structural Fe(II) in 0.5 M HCl had the same isotope composition as the edge plus structural Fe(II) in the NaH_2PO_4 extract (see SI for details of calculation and mass balance discussion).

During the initial, rapid stage of reduction, structural Fe(III) extracted by 0.5 M HCl was isotopically heavier than the starting bulk NAu-1 in all reduction experiments (stage 1, Figure 2), while all the δ^{56}Fe values of the different Fe(II) pools were lower than those of structural Fe(III). Basal-sorbed Fe(II) exhibited the most negative δ^{56}Fe values among all Fe(II) pools, with the lowest values observed when the extent of reduction was slightly above 2%. Edge plus structural Fe(II) generally had the heaviest Fe isotopic compositions of all the Fe(II) pools, while aqueous Fe(II) exhibited intermediate δ^{56}Fe values between those of basal and edge plus structural Fe(II). The isotopic Fe compositions of all three Fe(II) pools converged toward that of the starting bulk NAu-1 by the end of stage 1.

During the second stage of reduction, the Fe isotope composition of aqueous and basal-sorbed Fe(II) continued to become isotopically heavier, while that of edge plus structural Fe(II) decreased or remained constant (stage 2, Figure 2, SI Table S4). The final δ^{56}Fe values of aqueous and basal-sorbed Fe(II) were close to (*Geobacter* reactors, Figure 2B), or even higher than (*Shewanella* and chemical reactors, Figure 2A and C), that of the starting bulk clay. Meanwhile, the δ^{56}Fe values of edge plus structural Fe(II) and structural Fe(III) decreased with increasing extent of reduction (Figure 2) until, in the chemical reduction experiments, the two eventually reached identical δ^{56}Fe values below that of the starting bulk clay (Figure 2C). Although three chemical reactors in stage 2 were run at elevated temperature (70 °C) and one reactor at room temperature (SI Table S1), the general trends of the Fe isotope compositions were quite similar to those observed in the microbial reduction experiments (Figure 2).

Changes in Fe Isotope Composition during Clay−Fe(II) Exchange. In the exchange experiments, the Fe isotope compositions of the different Fe pools deviated from the δ^{56}Fe values of starting NAu-1 and aqueous Fe(II) after 30 and 57 days (Figure 3). Structural Fe extracted by 0.5 M HCl was isotopically heavier than the starting NAu-1. Aqueous and basal-sorbed Fe were isotopically lighter than the Fe(II) added at the start of the experiments, while NaH_2PO_4 extractable Fe was heavier. During the entire duration of the exchange experiments, pH remained stable at 6. The extent of atom

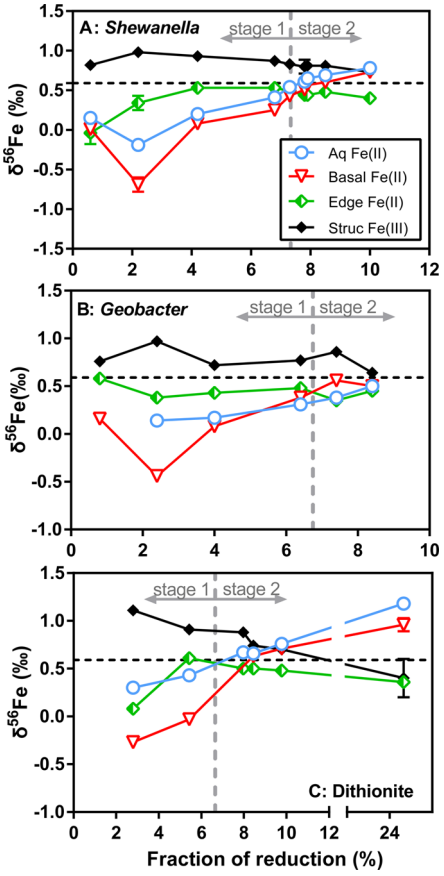

Figure 2. Iron isotope compositions of the different Fe(II) pools (aqueous, basal-sorbed, and edge plus structural sites) and structural Fe(III) in the 0.5 M HCl extracts (see SI for calculation of the latter) during NAu-1 reduction by *Shewanella* (A), *Geobacter* (B), and dithionite (C) under pH 6.8. Dashed horizontal lines indicate the original δ^{56}Fe value of bulk NAu-1, representing δ^{56}Fe of the starting structural Fe(III). Note that, during stage 2, aqueous Fe(II) becomes isotopically heavier than edge plus structural Fe(II). The transition from stage 1 to stage 2 is thus characterized by systematic changes in the biological reduction kinetics (see Figure 1) and the Fe isotopic signatures. Error bars indicate one standard deviation based on either duplicate reactors for microbial reduction experiments or repeated analyses for chemical reduction experiments.

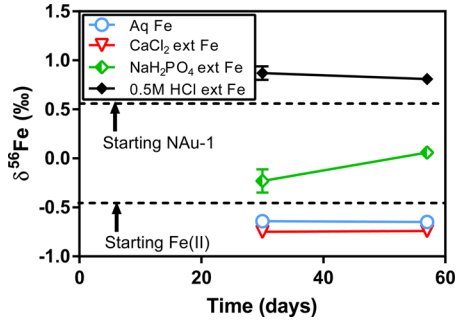

Figure 3. Iron isotope compositions of different Fe pools upon mixing of aqueous Fe(II) with NAu-1 (Fe molar ratio: 1:4, pH 6.0). The black horizontal lines indicate the starting δ^{56}Fe values of bulk NAu-1 and aqueous Fe(II), respectively. Error bars indicate one standard deviation based on two duplicate reactors and are smaller than symbol size when not shown.

DOI: 10.1021/acs.est.6b02019
Environ. Sci. Technol. 2016, 50, 8661−8669

exchange has been shown to be ca. 4% between aqueous Fe(II) and NAu-1 based on δ^{57}Fe values, which have been reported previously.[51] The δ^{56}Fe data for the same experiments have been first reported in the current study.

DISCUSSION

Two-Stage Microbial and Chemical Clay Reduction. We hypothesize that, in both the microbial and chemical reduction experiments, structural Fe reduction proceeds in two consecutive stages (SI Figure S4A-C). During stage 1, electrons are supplied to structural Fe(III) atoms in the edge sites of NAu-1. The resulting structural Fe(II) is released from the octahedral sheet and attaches to hydroxyl groups, producing edge-bound Fe(II). A small amount of Fe(II) is released to solution, and subsequently partially adsorbs onto basal planes (SI Figure S4A). Edge-bound and aqueous Fe(II) undergoes ETAE with structural Fe(III) located near to the clay particle edges. *Shewanella oneidensis*, which is able to release electron shuttling compounds,[52] reduces ~7% of total Fe(III) within 8 days (Figure 1C), while *G. sulfurreducens*, which does not release electron shuttling compounds and requires direct cell contact to mineral surfaces,[52] only achieves ~2% reduction after 126 days (Figure 1C). However, the extent of reduction by *G. sulfurreducens* increases rapidly to ~6% within 7 days after addition of AQDS as an exogenous electron shuttle.

When assessing the electron transfer pathways in our microbial reduction experiments, two models have been proposed by previous studies: a parallel-to-layer pathway initiating from the edge sites[18,19] vs both parallel-to-layer and perpendicular-to-layer through basal planes pathways.[53] Bishop et al.[53] used the correlation between the interlayer expandability and the extent of bioreduction to argue for possible perpendicular-to-layer electron transfer pathway during reduction by strain *Shewallena putrefaciens* CN32. This is inconsistent with prior Mössbauer work on bioreduced nontronite by *Shewallena oneidensis* MR-1, suggesting a parallel-to-layer pathway only.[18,19] Both differences in bacterial strains and heterogeneity of clay particles may account for the discrepancy observed in these studies.[53] It has also been shown that organic matter in the interlayer space hinders the extent and rate of bioreduction of nontronite NAu-2 by methanogens.[54] However, a recent Mössbauer study of bioreduced NAu-2 reveals that perpendicular-to-layer electron transfer occurs only with the assistance of AQDS and not with *Shewanella* alone.[55] Our limited extent of reduction argues for the dominance of the parallel-to-layer electron transfer pathway in the *Shewallena* experiments and the perpendicular-to-layer pathway may play a role in our *Geobacter* experiments with AQDS.

During stage 2, microbial reduction slows down significantly: the extent of reduction increases from 7% at day 8 to 10% at day 161 with *Shewanella*, and from 6% at day 162 to 8% at day 240 with *Geobacter*. Initial structural Fe(III) at edge sites (i.e., Fe(III) exposed to solution) of NAu-1 represents 2.7 to 13.6% of the total initial Fe(III) (considering particles ranging from 0.01 to 0.05 μm, see SI for details of calculation). Thus, only about 10% of the Fe(III) near the clay particle edges appears to be directly accessible to the iron-reducing bacteria. This pool constitutes the finite, bioavailable Fe(III) pool[5] (SI Figure S4B). The size of this bioavailable Fe(III) pool may differ for different clay minerals considering that clay particles are heterogeneous by nature in crystallinity, particle size, surface area, and expandability.[53,56] It is worthwhile to note that the extent and rate of bioreduction is also influenced by the energetics of the system, as shown by continuing reduction after addition of fresh cells to previously ceased bioreduction experiments.[56,57] In the chemical reduction experiments, dithionite, with its small molecular size, is able to diffuse into the interior of the clay structure along basal planes (SI Figure S4C), hence explaining the higher extents of reduction of total structural Fe(III) (up to 24%, SI Table S2). It is important to note that, overall, chemical reduction by dithionite proceeds markedly faster than reduction by the two iron-reducing bacteria. The same extent of reduction achieved within minutes by dithionite requires several days in the microbial reduction experiments.

Fe Isotope Compositions. The observed changes in Fe isotope compositions are consistent with the proposed two-stage mechanism for structural Fe(III) reduction shown diagrammatically in Figure 4 and SI Figure S4. When the extent of reduction is low (stage 1), the isotopically light aqueous Fe(II) argues for atom exchange with structural Fe(III) on the edge sites (Figure 4A and SI Figure S4A). In the absence of atom exchange, aqueous Fe(II) would be expected to inherit the δ^{56}Fe signature of the outmost structural Fe atoms upon reductive dissolution. Partial dissolution of the starting NAu-1 shows that the outermost Fe atoms near the clay particle edges are isotopically heavy, while those located in the interior of the clay particles are isotopically light (see SI Table S5), which may reflect the isotope heterogeneity of the clay particles. Thus, aqueous Fe(II) would have shown a more positive δ^{56}Fe value than the bulk clay (e.g., δ^{56}Fe $\geq$ 0.74‰ when dissolution $\leq$1.5%, see SI Table S5), which is not the case. The existence of atom exchange between aqueous Fe(II) and other Fe phases is consistent with a previous finding using enriched isotope tracers.[51] Neumann et al.[51] proposed that electron injection by sorbed Fe(II) at edge sites, followed by bulk electron conduction through the octahedral sheet, would connect oxidation of edge-bound Fe(II) with reduction of structural Fe(III) at spatially separated sites. Considering the much smaller pool of aqueous Fe(II) than edge-bound Fe(II) in our experiments, we hypothesize that ETAE between aqueous Fe(II) and structural Fe(III) occurs via a transient sorbed Fe(II) phase on edge sites, which may or may not be captured in the edge-bound Fe(II) extract.

For the same reason, edge plus structural Fe(II) would become isotopically heavy if only reduction (i.e., electron transfer) occurs without atom exchange. The observed isotopically light edge plus structural Fe(II) and isotopically heavy structural Fe(III) suggest that atom exchange is coupled with electron transfer (i.e., ETAE) during stage 1.

Basal-sorbed Fe(II) exhibits the most negative δ^{56}Fe values. We propose three hypotheses to explain the observed values: 1) kinetic adsorption of aqueous Fe(II) onto basal planes; 2) ETAE between basal-sorbed Fe(II) and structural Fe(III); and 3) partial oxidation of basal-sorbed Fe(II) due to electron transfer from sorbed Fe(II) to structural Fe(III). The first hypothesis may explain the lightest basal-sorbed Fe(II) when the extent of reduction is ca. 2% (Figure 2), consistent with a kinetic sorption producing isotopically heavy aqueous Fe(II) during interaction between aqueous Fe(II) and goethite.[58] However, isotope data of later time points (i.e., at day 161 in *Shewallena* experiments) still showed an isotopically lighter basal-sorbed Fe(II) than that of the aqueous Fe(II) (Figure 2), arguing against a kinetic effect to fully explain our observed data. Electron transfer from basal-sorbed Fe(II) to sturcutral Fe(III) has been demonstrated previously.[36] However, atom

DOI: 10.1021/acs.est.6b02019
Environ. Sci. Technol. 2016, 50, 8661−8669

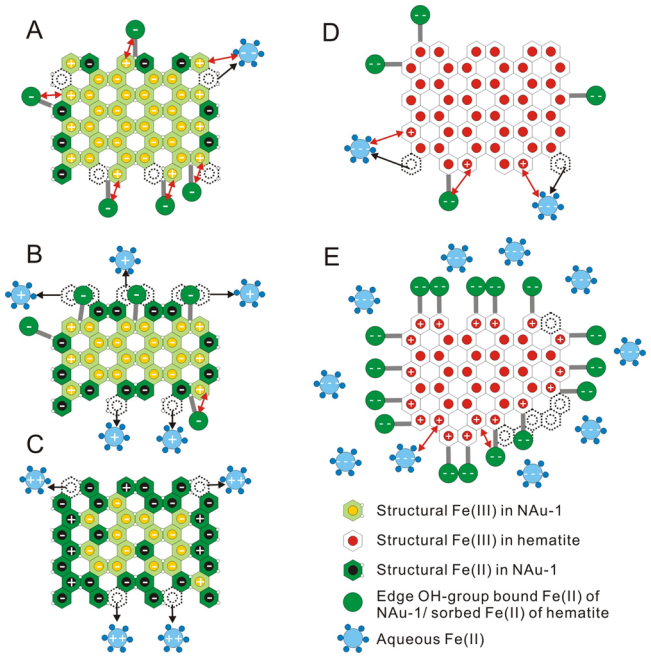

Figure 4. Comparison of reduction mechanisms of NAu-1 (top view) and hematite. (A) At low extent of reduction of NAu-1, the outmost structural Fe(III) is reduced by the bacteria (*Shewanella* and *Geobacter*) or dithionite to structural Fe(II). Fe(II) bound to edge hydroxyl groups and structural edge Fe(II) have the same isotope composition. The release of aqueous Fe(II) from structural Fe is indicated by the black arrow. ETAE between aqueous Fe(II) and structural Fe(III) and edge-bound Fe(II) and structural Fe(III) is shown by the red arrows. Basal-sorbed Fe(II) is not shown in the top view figures. (B) At high extent of reduction in biological experiments, residual heavy structural Fe(III) is reduced and dissolves, producing isotopically heavy aqueous phase Fe(II) (indicated by "+" and the black arrows). Edge sites are saturated with structural and edge-bound Fe(II), inhibiting further reduction. ETAE between aqueous Fe(II) and structural Fe(III) is blocked, with minor ETAE between edge-bound Fe(II) and structural Fe(III), as indicated by the red arrow. (C) At ∼ 24% reduction in chemical experiments, interior structural Fe(III) is reduced, with a small amount of the isotopically heavy outmost Fe(II) released to the aqueous phase (indicated by "++"). (D) For Fe oxyhydroxide minerals, reduction does not cause the accumulation of structural Fe(II). Both aqueous ("---" indicates lowest δ^{56}Fe) and adsorbed Fe(II) ("--" indicates lower δ^{56}Fe) undergo ETAE with structural Fe(III) on the mineral surfaces ("+" indicates high δ^{56}Fe). (E) When surface is saturated by sorbed Fe(II), no blockage of ETAE occurs due to lack of structural Fe(II), thus maintaining isotopic equilibrium.

exchange has never been shown to occur between basal-sorbed Fe(II) and structural Fe(III), presumably due to physical blockage by a tetrahedral sheet between the two. Thus, we reject the second hypothesis. Meanwhile, if basal-sorbed Fe(II) was partially oxidized to Fe(III), then residual Fe(II) will be isotopically lighter than the original sorbed Fe(II),[59,60] which presumably had a similar isotope composition with the aqueous Fe(II). Due to the small quantity of this Fe(III) product, our $CaCl_2$ extraction and/or the Ferrozine method may fail to recover this Fe(III) phase. This third one remains a viable hypothesis to be tested further.

During stage 2, the progressively heavier isotopic compositions of aqueous and basal-sorbed Fe(II) (Figure 2) are explained by the continued reductive dissolution of the outermost pool of structural Fe(III) and the cessation of ETAE between aqueous Fe(II) and structural Fe(III). During this stage, some ETAE between edge-bound Fe(II) and adjacent structural Fe(III) is still possible, due to close site contact, but not between aqueous Fe(II) and structural Fe(III) (Figure 4B and SI Figure S4B). In other words, the accumulation of structural Fe(II) along the edges of the clay particles causes the blocking of ETAE.

Compared to the near-edge, bioavailable Fe(III) pool, the interior Fe(III) pool is not accessible to the bacteria. The small dithionite molecules, however, are able to further reduce a significant portion of the interior Fe(III) pool (Figure 4C and SI Figure S4C). The aqueous and basal-sorbed Fe(II) thus derives from the reductive dissolution of a relatively small portion of the outermost component of the Fe(III) pool with δ^{56}Fe values of ∼1‰ (SI Table S4). Structural Fe(II) and structural Fe(III) are both isotopically light (Figures 2C and 4C), reflecting the inheritance of the light δ^{56}Fe values of the bulk interior Fe(III) pool, without ETAE (see SI Table S5). Alternatively, the aqueous plus basal-sorbed Fe(II) could become enriched in heavy Fe isotopes due to the precipitation of an isotopically light secondary mineral phase during stage 2. However, no secondary mineral precipitates could be detected by SEM in all the reduced samples, even at the highest extents of Fe(III) reduction (SI Figure S6).

Fe Isotope Fractionations. With the exception of the initial data points, the Fe isotope fractionation factors in the microbial and chemical reduction experiments generally decrease with increasing extent of reduction during stage 1 (Figure 5 and SI Figure S7, Table S4). The fractionation factors between edge plus structural Fe(II) and structural Fe(III) on the one hand (Figure 5A), and the combined Fe(II) pools and structural Fe(III) on the other (SI Figure S7), both decrease from −1.0 to −0.3‰; their near identical trends reflect the dominant contribution of edge plus near-edge structural Fe(II)

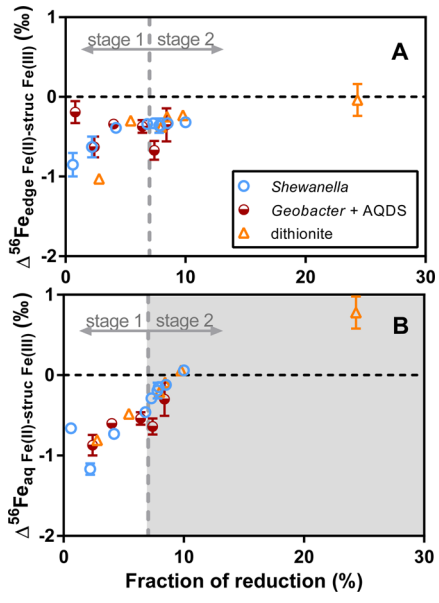

Figure 5. Changes in the Fe isotope fractionation factors $\Delta^{56}Fe_{edge\ Fe(II)\text{-}struc\ Fe(III)}$ (panel A) and $\Delta^{56}Fe_{aq\ Fe(II)\text{-}struc\ Fe(III)}$ (panel B) in biological and chemical reduction experiments plotted against the extent of reduction. The vertical lines indicate the transition from stage 1 to stage 2. The gray background in stage 2 of panel B shows that no ETAE occurs between aqueous Fe(II) and structural Fe(III). Error bars indicate one standard deviation of propagated errors.

DOI: 10.1021/acs.est.6b02019
Environ. Sci. Technol. 2016, 50, 8661−8669

to total Fe(II). The decreasing trends are explained by the finite size of the bioavailable Fe(III) pool. At the onset of reduction, the fractionation factors are the largest due to extensive ETAE. With reduction proceeding, edge sites are progressively occupied by Fe(II), resulting in less structural Fe(III) available for ETAE, and the fractionation factors decrease. In all the reduction experiments, the maximum fractionation factors are observed for $\Delta^{56}Fe_{aq\ Fe(II)\text{-}struc\ Fe(III)}$ (−1.2 to −0.8‰) when the extent of reduction is small, ca. 2% (Figure 5B). These large values reflect extensive ETAE between aqueous Fe(II) and structural Fe(III) assisted by dynamic sorption/desorption via a transient sorbed Fe(II) phase (Figure 4A and SI Figure S4A).

During stage 2, as the finite bioavailable Fe(III) pool is nearly exhausted, the reduction rates in the *Shewanella* reactors drop to very low values, while the $\Delta^{56}Fe_{struc\ Fe(II)\text{-}struc\ Fe(III)}$ values stabilize at −0.34 ± 0.02‰ (Figure 5A), reflecting minor ETAE between edge-bound Fe(II) and structural Fe(III) (Figure 4B andSI Figure S4B). In the experiments with dithionite, much faster reduction ultimately results in $\Delta^{56}Fe_{struc\ Fe(II)\text{-}struc\ Fe(III)}$ values of ∼0‰ (Figure 5A), while the extent of reduction reaches 24%. The net zero isotopic fractionation implies that 100% of the structural Fe(III) pool accessible to dithionite has been reduced at that point.

In the microbial reduction experiments, fractionation factors between aqueous Fe(II) and structural Fe(III) change from −0.3‰ to 0.1‰ during stage 2 (Figure 5B), which signals the progressive cessation of ETAE and the cumulative release of isotopically heavy Fe to solution (Figure 4B and SI Figure S4B). When the two phases coincidentally attain the same isotopic composition, the bioavailable Fe(III) pool is completely consumed. At the end of the chemical reduction experiments, that is, at 24% reduction, the $\Delta^{56}Fe_{aq\ Fe(II)\text{-}struc\ Fe(III)}$ value has become positive due to the absence of atom exchange between aqueous Fe(II) and structural Fe(III) and between aqueous Fe(II) and structural Fe(II). At this stage, all the edge sites are saturated with Fe(II) and a lack of atom exchange between aqueous Fe(II) and structural Fe(II) indicates that atom exchange must be coupled with electron transfer. Facilitation of atom exchange by electron transfer has been shown previously by the higher extent of atom exchange for interactions between aqueous Fe(II) and Fe oxyhydroxides than between aqueous Fe(III) and amorphous Fe oxide.[28] This in turn demonstrates that ETAE is the key mechanism for Fe isotope fractionation during the first stage of clay reduction (Figure 4A and SI Figure S4A).

Comparison to Fe(II)-NAu-1 Exchange Experiments. Similar to the stage 1 results of the microbial and chemical reduction experiments, the mixing of aqueous Fe(II) and NAu-1 produces structural Fe(III) that is isotopically heavier than the starting clay material, as well as isotopically light Fe(II) (Figure 3). However, the relatively constant isotopic compositions and fractionation factors during the exchange experiments contrast with the time-dependent trends seen in the reduction experiments. A previous study has shown that mixing aqueous Fe(II) and NAu-1 at pH 6 causes ∼3% reduction of structural Fe(III).[33] The isotope fractionation factors in the mixing experiments are in general comparable to those of the reduction experiments at ∼3% extent of reduction (SI Table S4). Due to the small extent of reduction, only limited structural Fe(II) is generated and no saturation of edge sites over time would occur in the mixing experiments. The invariant isotope fractionation factors with time imply a constant extent of ETAE throughout the mixing experiments. The small differences between the fractionation factors observed in the exchange and reduction experiments (SI Table S4) could be due to differences in the amounts of Fe(II) sorbed onto basal and edge sites because of pH differences (6.0 in exchange experiments versus 6.8 in reduction experiments).[36]

Iron Reduction in Clay Mineral Versus Fe(III) Oxyhydroxides. The in situ reduction of structural Fe(III) which leads to the blocking of ETAE between aqueous Fe(II) and structural Fe(III) is unique to clay minerals with layered structure, and distinct from Fe(III) oxyhydroxide mineral reduction. Before the bioavailable finite Fe(III) pool is exhausted, ETAE mainly takes place between edge-bound Fe(II) and structural Fe(III), as well as between aqueous Fe(II) and structural Fe(III) (Figure 4A). With the accumulation of structural Fe(II), the amount of structural Fe(III) available for ETAE with aqueous Fe(II) decreases. Ultimately, ETAE with the interior structural Fe(III) pool ceases (Figure 4B and SI Figure S4B). Basal-sorbed Fe(II) does not undergo ETAE with structural Fe(III) due to the physical separation by the tetrahedral sheets (SI Figure S4A). In contrast, Fe(II) produced during the reduction of Fe(III) oxyhydroxides mainly ends up in the aqueous and adsorbed phases (Figure 4D). Even when the surface of the Fe(III) oxyhydroxide mineral is saturated with adsorbed Fe(II), structural Fe(III) remains available to ETAE with aqueous and adsorbed Fe(II), due to the lack of blockage by structural Fe(II) (Figure 4E). Thus, aqueous Fe(II) can maintain isotopic equilibrium with solid-phase Fe(III) and remain isotopically lighter than sorbed Fe(II).[27,30,31]

Our results imply that Fe isotope fractionations can potentially yield signatures that may allow one to distinguish reduction of structural Fe(III) in layered clay minerals by dissimilatory iron reducing bacteria from reduction of Fe(III) oxyhydroxides in reducing environments. When most bioavailable Fe(III) in clays is exhausted, microbial reduction becomes inhibited due to site saturation, and further ETAE between aqueous Fe(II) and structural Fe(III) no longer takes place. The complete conversion of bioavailable Fe(III) to Fe(II) in clay (zero fractionation between aqueous phase and structural Fe(III) in mineral), coupled with limited reductive dissolution (∼1%), indicates that Fe redox cycling mediated by microbes may be an isotopically reversible process. This conclusion is consistent with recent bulk measurements of clay redox speciation which indicate that ferruginous clay may serve as a rechargeable energy source for bacteria in soils and sediments.[55] The blockage of ETAE will likely also influence the reactivity of edge plus structural Fe(II) toward nutrients and contaminants, which warrants further exploration.

The Fe isotope compositions of major Fe-bearing minerals (i.e., magnetite, siderite) in the Banded Iron Formations in the rock record have been interpreted as biosignatures of dissimilatory iron reduction (DIR) of Fe(III) oxyhydroxides either in situ[61−63] in the sediments or through a benthic shuttle.[64,65] This interpretation is largely based on the generation of isotopically light Fe(II) by DIR of Fe(III) oxyhydroxides as demonstrated in numerous experimental studies.[29−31] Our findings here imply that Fe bearing clay minerals may not serve as a faithful recorder of microbial activities (i.e., DIR) on ancient Earth. If bioavailable Fe was exhausted during microbial reduction, no distinctive Fe isotope signature would be detected for the end product ferrous phases when analyzing clay minerals in the rock record. On the other

DOI: 10.1021/acs.est.6b02019
Environ. Sci. Technol. 2016, 50, 8661−8669

hand, a lack of isotope discrepancy between ferrous and ferric phases associated with clay minerals cannot be used to rule out the existence of microbial activities.

■ ASSOCIATED CONTENT

Supporting Information

The Supporting Information is available free of charge on the ACS Publications website at DOI: 10.1021/acs.est.6b02019.

Additiional information as noted in the text (PDF)

■ AUTHOR INFORMATION

Corresponding Author

*Phone: 1-519-888-4567 ext. 33235; fax: 1-519-746-7484; e-mail: lingling.wu@uwaterloo.ca.

Notes

The authors declare no competing financial interest.

■ ACKNOWLEDGMENTS

We are deeply indebted for data on exchange experiments and insightful comments provided by Anke Neumann and Michelle Scherer (University of Iowa). Funding for this work was provided by an Ontario Early Researcher Award and NSERC Discovery grant awarded to LW, the NASA Astrobiology Institute, and the Canada Excellence Research Chair (CERC) program.

■ REFERENCES

(1) Stucki, J. W.; Faïza Bergaya, B. K. G. T. a. G. L., Chapter 8 Properties and Behaviour of Iron in Clay Minerals. In *Developments in Clay Science*; Elsevier, 2006; Vol. *1*, pp 423−475.

(2) Hofstetter, T. B.; Neumann, A.; Schwarzenbach, R. P. Reduction of nitroaromatic compounds by Fe(II) species associated with iron-rich smectites. *Environ. Sci. Technol.* **2006**, *40* (1), 235−242.

(3) Peretyazhko, T. S.; Zachara, J. M.; Kukkadapu, R. K.; Heald, S. M.; Kutnyakov, I. V.; Resch, C. T.; Arey, B. W.; Wang, C. M.; Kovarik, L.; Phillips, J. L.; Moore, D. A. Pertechnetate (TcO_4^-) reduction by reactive ferrous iron forms in naturally anoxic, redox transition zone sediments from the Hanford Site, USA. *Geochim. Cosmochim. Acta* **2012**, *92* (0), 48−66.

(4) Wu, L. M.; Zhou, C. H.; Keeling, J.; Tong, D. S.; Yu, W. H. Towards an understanding of the role of clay minerals in crude oil formation, migration and accumulation. *Earth-Sci. Rev.* **2012**, *115* (4), 373−386.

(5) Jaisi, D. P.; Kukkadapu, R. K.; Eberl, D. D.; Dong, H. Control of Fe(III) site occupancy on the rate and extent of microbial reduction of Fe(III) in nontronite. *Geochim. Cosmochim. Acta* **2005**, *69* (23), 5429−5440.

(6) Stucki, J. W., Properties and behaviour of iron in clay minerals. In *Handbook of Clay Science*; Bergaya, F.; Theng, B. K. G.; Lagaly, G., Eds.; Elsevier: Boston, 2006.

(7) Stucki, J. W. A review of the effects of iron redox cycles on smectite properties. *C. R. Geosci.* **2011**, *343* (2−3), 199−209.

(8) Stucki, J. W.; Lee, K.; Zhang, L.; Larson, R. A. Effects of iron oxidation state on the surface and structural properties of smectites. *Pure Appl. Chem.* **2002**, *74* (11), 2145−2158.

(9) Stucki, J. W.; Tessier, D. Effects of iron oxidation state on the texture and structural order of Na-nontronite Gels. *Clays Clay Miner.* **1991**, *39* (2), 137−143.

(10) Abollino, O.; Aceto, M.; Malandrino, M.; Sarzanini, C.; Mentasti, E. Adsorption of heavy metals on Na-montmorillonite. Effect of pH and organic substances. *Water Res.* **2003**, *37* (7), 1619−1627.

(11) Catalano, J. G.; Brown, G. E. Uranyl adsorption onto montmorillonite: Evaluation of binding sites and carbonate complexation. *Geochim. Cosmochim. Acta* **2005**, *69* (12), 2995−3005.

(12) Haderlein, S. B.; Weissmahr, K. W.; Schwarzenbach, R. P. Specific adsorption of nitroaromatic: explosives and pesticides to clay minerals. *Environ. Sci. Technol.* **1996**, *30* (2), 612−622.

(13) Kostka, J. E.; Haefele, E.; Viehweger, R.; Stucki, J. W. Respiration and dissolution of iron(III)- containing clay minerals by bacteria. *Environ. Sci. Technol.* **1999**, *33*, 3127−3133.

(14) Kostka, J. E.; Wu, J.; Nealson, K. H.; Stucki, J. W. The impact of structural Fe(III) reduction by bacteria on the surface chemistry of smectite clay minerals. *Geochim. Cosmochim. Acta* **1999**, *63* (22), 3705−3713.

(15) Dong, H.; Kostka, J. E.; Kim, J. Microscopic Evidence for Microbial Dissolution of Smectite. *Clays Clay Miner.* **2003**, *51* (5), 502−512.

(16) Stucki, J. W.; Lee, K.; Zhang, L.; Larson, R. A. Effects of iron oxidation state on the surface and structural properties of smectites. *Pure Appl. Chem.* **2002**, *74* (11), 2145−2158.

(17) Dong, H. L.; Jaisi, D. P.; Kim, J.; Zhang, G. X. Microbe-clay mineral interactions. *Am. Mineral.* **2009**, *94* (11−12), 1505−1519.

(18) Ribeiro, F. R.; Fabris, J. D.; Kostka, J. E.; Komadel, P.; Stucki, J. W. Comparisons of structural iron reduction in smectites by bacteria and dithionite: II. A variable-temperature Mossbauer spectroscopic study of Garfield nontronite. *Pure Appl. Chem.* **2009**, *81* (8), 1499−1509.

(19) Komadel, P.; Madejova, J.; Stucki, J. W. Structural Fe(III) reduction in smectites. *Appl. Clay Sci.* **2006**, *34* (1−4), 88−94.

(20) Lee, K.; Kostka, J. E.; Stucki, J. W. Comparisons of structural Fe reduction in smectites by bacteria and dithionite: An infrared spectroscopic study. *Clays Clay Miner.* **2006**, *54* (2), 195−208.

(21) Kashefi, K.; Shelobolina, E. S.; Elliott, W. C.; Lovley, D. R. Growth of Thermophilic and Hyperthermophilic Fe(III)-Reducing Microorganisms on a Ferruginous Smectite as the Sole Electron Acceptor. *Appl. Environ. Microbiol.* **2008**, *74* (1), 251−258.

(22) Kostka, J. E.; Haefele, E.; Viehweger, R.; Stucki, J. W. Respiration and dissolution of iron(III)-containing clay minerals by bacteria. *Environ. Sci. Technol.* **1999**, *33* (18), 3127−3133.

(23) Kim, J.; Dong, H. L.; Seabaugh, J.; Newell, S. W.; Eberl, D. D. Role of microbes in the smectite-to-Illite reaction. *Science* **2004**, *303*, 830−832.

(24) Johnson, C. M.; Beard, B. L.; Roden, E. E. The iron isotope fingerprints of redox and biogeochemical cycling in modern and ancient Earth. *Annu. Rev. Earth Planet. Sci.* **2008**, *36*, 457−493.

(25) Hofmann, A.; Bekker, A.; Rouxel, O.; Rumble, D.; Master, S. Multiple sulphur and iron isotope composition of detrital pyrite in Archaean sedimentary rocks: A new tool for provenance analysis. *Earth Planet. Sci. Lett.* **2009**, *286* (3−4), 436−445.

(26) Nishizawa, M.; Yamamoto, H.; Ueno, Y.; Tsuruoka, S.; Shibuya, T.; Sawaki, Y.; Yamamoto, S.; Kon, Y.; Kitajima, K.; Komiya, T.; Maruyama, S.; Hirata, T. Grain-scale iron isotopic distribution of pyrite from Precambrian shallow marine carbonate revealed by a femto-second laser ablation multicollector ICP-MS technique: Possible proxy for the redox state of ancient seawater. *Geochim. Cosmochim. Acta* **2010**, *74* (9), 2760−2778.

(27) Crosby, H. A.; Johnson, C. M.; Roden, E. E.; Beard, B. L. Coupled Fe(II)-Fe(III) electron and atom exchange as a mechanism for Fe isotope fractionation during dissimilatory iron oxide reduction. *Environ. Sci. Technol.* **2005**, *39*, 6698−6704.

(28) Wu, L.; Percak-Dennett, E. M.; Beard, B. L.; Roden, E. E.; Johnson, C. M. Stable iron isotope fractionation between aqueous Fe(II) and model Archean ocean Fe-Si coprecipitates and implications for iron isotope variations in the ancient rock record. *Geochim. Cosmochim. Acta* **2012**, *84* (0), 14−28.

(29) Crosby, H. A.; Roden, E. E.; Johnson, C. M.; Beard, B. L. The mechanisms of iron isotope fractionation produced during dissimilatory Fe(III) reduction by *Shewanella putrefaciens* and *Geobacter sulfurreducens*. *Geobiology* **2007**, *5*, 169−189.

(30) Percak-Dennett, E. M.; Roden, E. E.; Beard, B. L.; Johnson, C. M. Iron isotope fractionation during dissimilatory iron reduction under simulated Archean conditions. *Geobiology* **2011**, *9* (3), 205−220.

DOI: 10.1021/acs.est.6b02019
Environ. Sci. Technol. 2016, 50, 8661−8669

(31) Wu, L.; Beard, B. L.; Roden, E. E.; Johnson, C. M. Influence of pH and dissolved Si on Fe isotope fractionation during dissimilatory microbial reduction of hematite. *Geochim. Cosmochim. Acta* **2009**, *73* (19), 5584−5599.
(32) Beard, B. L.; Handler, R. M.; Scherer, M. M.; Wu, L.; Czaja, A. D.; Heimann, A.; Johnson, C. M. Iron isotope fractionation between aqueous ferrous iron and goethite. *Earth Planet. Sci. Lett.* **2010**, *295* (1−2), 241−250.
(33) Skulan, J. L.; Beard, B. L.; Johnson, C. M. Kinetic and equilibrium Fe isotope fractionation between aqueous Fe(III) and hematite. *Geochim. Cosmochim. Acta* **2002**, *66* (17), 2995−3015.
(34) Wu, L.; Beard, B. L.; Roden, E. E.; Johnson, C. M. Stable iron isotope fractionation between aqueous Fe(II) and hydrous ferric oxide. *Environ. Sci. Technol.* **2011**, *45* (5), 1847−1852.
(35) Keeling, J. L.; Raven, M. D.; Gates, W. P. Geology and characterization of two hydrothermal nontronites from weathered metamorphic rocks at the Uley graphite mine, South Australia. *Clays Clay Miner.* **2000**, *48* (5), 537−548.
(36) Neumann, A.; Olson, T. L.; Scherer, M. M. Spectroscopic evidence for Fe(II)-Fe(III) electron transfer at clay mineral edge and basal sites. *Environ. Sci. Technol.* **2013**, *47* (13), 6969−6977.
(37) Jackson, M. L. *Soil Chemical Analysis: Advanced Course*; Madison, WI, 1956.
(38) Myers, C. R.; Nealson, K. H. Bacterial manganese reduction and growth with manganese oxide as the sole electron acceptor. *Science* **1988**, *240*, 1319−1321.
(39) Caccavo, F.; Lonergan, D. J.; Lovley, D. R.; Davis, M.; Stolz, J. F.; McInerney, M. J. Geobacter sulfurreducens sp. nov., a hydrogen- and acetate-oxidizing dissimilatory metal-reducing microorganism. *Appl. Environ. Microbiol.* **1994**, *60*, 3752−3759.
(40) Luan, F.; Gorski, C. A.; Burgos, W. D. Thermodynamic controls on the microbial reduction of iron-bearing nontronite and uranium. *Environ. Sci. Technol.* **2014**, *48* (5), 2750−2758.
(41) Bergaya, F.; Lagaly, G.; Vayer, M., Chapter 12.10 Cation and Anion Exchange. In *Developments in Clay Science*; Bergaya, F.; Theng, B. K. G.; Lagaly, G., Eds. Elsevier, 2006; Vol. *1*, pp 979−1001.
(42) Schoonheydt, R. A.; Johnston, C. T., Chapter 3 Surface and Interface Chemistry of Clay Minerals. In *Developments in Clay Science*; Bergaya, F.; Theng, B. K. G.; Lagaly, G., Eds.; Elsevier, 2006; Vol. *1*, pp 87−113.
(43) Amonette, J. E.; Templeton, J. C. Improvements to the quantitative assay of nonrefractory minerals for Fe (II) and total Fe using 1, 10-phenanthroline. *Clays Clay Miner.* **1998**, *46* (1), 51−62.
(44) Stookey, L. L. Ferrozine- A New Spectrophotometric Reagent for Iron. *Anal. Chem.* **1970**, *42* (7), 779−781.
(45) Schilt, A. A. *Analytical Application of 1, 10- Phenanthroline and Related Compounds*. Pergamon Press: Oxford; New York, 1969; Vol. *32*.
(46) Clesceri, L. S.; Greenberg, A. E.; Eaton, A. D. *Standard Methods for the Examination of Water and Wastewater*. American Public Health Association: Washington, D. C., 1989.
(47) Beard, B. L.; Johnson, C. M.; Skulan, J. L.; Nealson, K. H.; Cox, L.; Sun, H. Application of Fe isotopes to tracing the geochemical and biological cycling of Fe. *Chem. Geol.* **2003**, *195* (1−4), 87−117.
(48) Kloprogge, J. T.; Komarneni, S.; Amonette, J. E. Synthesis of smectite clay minerals: a critical review. *Clays Clay Miner.* **1999**, *47* (5), 529−554.
(49) Weinrach, J.; Meyer, D.; Guy, J., Jr.; Michalski, P.; Carter, K.; Grubisha, D.; Bennett, D. A structural study of sodium dithionite and its ephemeral dihydrate: A new conformation for the dithionite ion. *J. Crystallogr. Spectrosc. Res.* **1992**, *22* (3), 291−301.
(50) Meunier, A. *Clays*. Springer: 2005; p 467.
(51) Neumann, A.; Wu, L.; Li, W.; Beard, B. L.; Johnson, C. M.; Rosso, K. M.; Frierdich, A. J.; Scherer, M. M. Atom Exchange between Aqueous Fe(II) and Structural Fe in Clay Minerals. *Environ. Sci. Technol.* **2015**, *49* (5), 2786−2795.
(52) Nevin, K. P.; Lovley, D. R. Mechanisms for Fe(III) oxide reduction in sedimentary environments. *Geomicrobiol. J.* **2002**, *19*, 141−159.
(53) Bishop, M. E.; Dong, H.; Kukkadapu, R. K.; Liu, C.; Edelmann, R. E. Bioreduction of Fe-bearing clay minerals and their reactivity toward pertechnetate (Tc-99). *Geochim. Cosmochim. Acta* **2011**, *75* (18), 5229−5246.
(54) Zhang, J.; Dong, H.; Zeng, Q.; Agrawal, A. The role of Fe(III) bioreduction by methanogens in the preservation of organic matter in smectite. *Chem. Geol.* **2014**, *389* (0), 16−28.
(55) Zhao, L.; Dong, H.; Kukkadapu, R. K.; Zeng, Q.; Edelmann, R. E.; Pentrák, M.; Agrawal, A. Biological Redox Cycling of Iron in Nontronite and Its Potential Application in Nitrate Removal. *Environ. Sci. Technol.* **2015**, *49* (9), 5493−5501.
(56) Jaisi, D. P.; Dong, H.; Liu, C. Influence of biogenic Fe(II) on the extent of microbial reduction of Fe(III) in clay minerals nontronite, Illite, and chlorite. *Geochim. Cosmochim. Acta* **2007**, *71* (5), 1145−1158.
(57) Jaisi, D. P.; Dong, H.; Plymale, A. E.; Fredrickson, J. K.; Zachara, J. M.; Heald, S.; Liu, C. Reduction and long-term immobilization of technetium by Fe(II) associated with clay mineral nontronite. *Chem. Geol.* **2009**, *264* (1−4), 127−138.
(58) Reddy, T. R.; Frierdich, A. J.; Beard, B. L.; Johnson, C. M. The effect of pH on stable iron isotope exchange and fractionation between aqueous Fe(II) and goethite. *Chem. Geol.* **2015**, *397*, 118−127.
(59) Beard, B. L.; Johnson, C. M. Fe isotope variations in the modern and ancient earth and other planetary bodies. *Rev. Mineral. Geochem.* **2004**, *55* (1), 319−357.
(60) Wu, L.; Brucker, R. P.; Beard, B. L.; Roden, E. E.; Johnson, C. M. Iron isotope characteristics of hot springs at Chocolate Pots, Yellowstone National Park. *Astrobiology* **2013**, *13* (11), 1091−1101.
(61) Craddock, P. R.; Dauphas, N. Iron and carbon isotope evidence for microbial iron respiration throughout the Archean. *Earth Planet. Sci. Lett.* **2011**, *303* (1−2), 121−132.
(62) Heimann, A.; Johnson, C. M.; Beard, B. L.; Valley, J. W.; Roden, E. E.; Spicuzza, M. J.; Beukes, N. J. Fe, C, and O isotope compositions of banded iron formation carbonates demonstrate a major role for dissimilatory iron reduction in ∼ 2.5 Ga marine environments. *Earth Planet. Sci. Lett.* **2010**, *294* (1−2), 8−18.
(63) Johnson, C. M.; Beard, B. L.; Klein, C.; Beukes, N. J.; Roden, E. E. Iron isotopes constrain biologic and abiologic processes in banded iron formation genesis. *Geochim. Cosmochim. Acta* **2008**, *72* (1), 151−169.
(64) Czaja, A. D.; Johnson, C. M.; Beard, B. L.; Eigenbrode, J. L.; Freeman, K. H.; Yamaguchi, K. E. Iron and carbon isotope evidence for ecosystem and environmental diversity in the ∼ 2.7 to 2.5 Ga Hamersley Province, Western Australia. *Earth Planet. Sci. Lett.* **2010**, *292* (1−2), 170−180.
(65) Severmann, S.; Lyons, T. w.; Anbar, A.; McManus, J.; Gordon, G. Modern iron isotope perspective on the benthic iron shuttle and the redox evolution of ancient oceans. *Geology* **2008**, *36* (6), 487−490.

DOI: 10.1021/acs.est.6b02019
Environ. Sci. Technol. 2016, 50, 8661−8669